Computational Materials Science 198 (2021) 110690

Contents lists available at ScienceDirect

Computational Materials Science

journal homepage: www.elsevier.com/locate/commatsci

Thermomechanical fatigue life due to scatter in constitutive parameters

Daniel Leidermark [a,*], James Rouse [b], Benedikt Engel [b], Christopher Hyde [b], Stephen Pattison [c], Svjetlana Stekovic [d]

[a] Division of Solid Mechanics, Linköping University, SE-58183 Linköping, Sweden
[b] Gas Turbine and Transmission Research Centre, University of Nottingham, NG7 2RD, United Kingdom
[c] Rolls-Royce plc, Elton Road, Derby DE24 8BJ, United Kingdom
[d] Division of Engineering Materials, Linköping University, SE-58183 Linköping, Sweden

ARTICLE INFO

Keywords:
Monte-Carlo analysis
Singular value decomposition
Thermomechanical fatigue
Nickel-base superalloy
Fatigue damage accumulation model

ABSTRACT

For critical component application, such as aerospace turbine rotors, it is imperative to be able to make accurate in-service material behaviour and component life predictions for both design and monitoring of component life. The development of such predictive capability is dependent on the quality of the experimental data from which the material parameters are derived. This paper shows the effect that scatter which may be present within experimental data, manifesting itself within the constitutive parameters derived from this data, has on the resulting fatigue crack initiation life of the nickel-based superalloy RR1000. Industrial relevance was added to this investigation by the use of flight representative thermomechanical fatigue loading cycles and state of the art material behaviour and fatigue crack initiation models used within the finite element simulations conducted. The effect of the ‘scatter in’ to the modelling approach on the outcoming predictions is made via a Monte-Carlo analysis. This analysis consisted of running the same simulation several times, but with the experimentally determined and validated ‘baseline’ constitutive parameters varied via correction factors built into the model, for each run via a singular value decomposition procedure. It was found that small ‘scatter in’ has only a very localised ‘scatter out’ effect on the crack initiation predictions under the flight representative loading.

1. Introduction

Thermomechanical fatigue (TMF) is one of the most damaging load conditions that can arise in hot gas turbine components. Therefore, accurate predictions of the onset of fatigue crack initiation and subsequent crack propagation are of high interest for the gas turbine industry, where gas turbines nowadays need to be designed for more frequent loadings and longer in-service lives to handle increasing amount of renewables and global increase in air travel.

Traditionally, a way of evaluating crack initiation life in a component is to post-process the results obtained in a finite element (FE) analysis. This is usually done by extracting a set of internal variables at a stable state and predict the number of cycles to crack initiation according to some defined life function that has previously been calibrated to experiments. This life function can be some kind of Coffin-Manson [1,2] or Morrow [3] type of expression. A method of distinguishing the most severely damaged location and orientation under multiaxial loading conditions is the so called critical-plane approach, trailing back to Findley [4]. An overview of different critical-plane approaches can *e.g.* be found in Karolczuk and Macha [5]. Bonnand et al. [6] used the critical-plane approach to evaluate fatigue life of a turboengine disc alloy undergoing multiaxial loadings. Another commonly used crack initiation model is the energy-based Smith-Watson-Topper model [7], accounting for mean stress influence by assuming that damage is brought on by the maximum tensile stress. Furthermore, the energy–density model introduced by Ostergren [8] was used for low-cycle fatigue with dwell time at elevated temperatures, where damage is assumed to be caused by plastic deformation at tensile loading. Kulawinski et al. [9] showed that both the Smith-Watson-Topper model and the Ostergren model were able to satisfactory predict the TMF life of Waspaloy, with a slightly better prediction using the Ostergren model. Furthermore, the well used critical-plane model by Fatemi and Socie [10] is based on the normal stress and shear strain, which handles mean stress and non-proportional loading effects.

Instead of using a post-processing method, another way can be to incorporate a fatigue damage parameter directly in the FE-analysis, and

* Corresponding author.
E-mail address: daniel.leidermark@liu.se (D. Leidermark).

https://doi.org/10.1016/j.commatsci.2021.110690
Received 14 December 2020; Received in revised form 11 June 2021; Accepted 25 June 2021

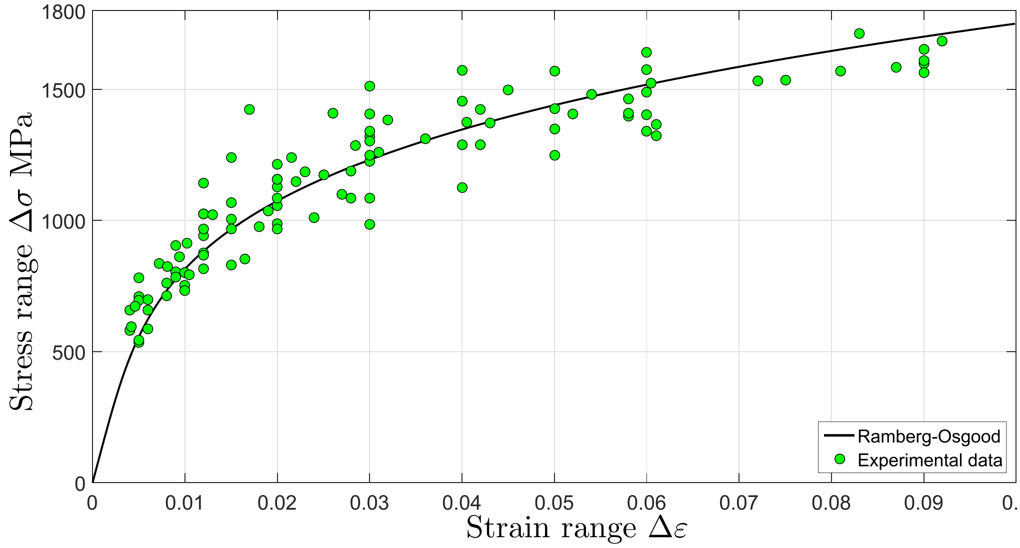

Fig. 1. Fictitious scatter of a material behaviour with an Ramberg–Osgood baseline constitutive representation.

incrementally accumulate damage until crack initiation occurs. Hence, closely linked to the constitutive model or directly implemented in a user-defined material model. Polák and Man [11] observed that fatigue crack initiation is related to early surface damage, where extrusions and intrusions form sharp surface crack-like defects [12] and by slip irreversibility [13]. Thus, indicating that fatigue crack initiation is attributed to the surface condition and its evolution. Hence, a variable that can, for instance, be incorporated in the user-defined material model to update the surface damage is desired, generating an even closer coupling between the microstrutural surface evolution and the classical continuum mechanics based constitutive modelling approach. A kinetic law of damage evolution was adopted by Lemaitre and Sermage [14] to be able to predict the fatigue crack initiation in a structure. The model is based on an isotropic scalar damage variable that defines crack initiation at a critical value through use of the accumulated plastic strain and the strain energy density release rate. The model is based on continuum damage mechanics and is coupled to the stress update, see *e.g.* [15]. Another damage approach, proposed for high-cycle fatigue loading is the one proposed by Ottosen et al. [16], which is based on the load history by defining an endurance surface, that translates with the loading using a "back-stress" term. The model was modified by Lindström [17] by use of a quadratic endurance surface instead of a linear one to induce an elliptical Haigh-diagram to be more consistent with experimental fatigue lives for ductile materials. A continuum damage approach based on the evolution of the associated endurance function defines the acquired damage, which eventually gives failure. The memory surface concept, first introduced in cyclic plasticity by Chaboche et al. [18] and is analogous to the yield surface in plasticity, was used by Jiang [19] to model the fatigue crack initiation behaviour under multiaxial loading by a plastic strain energy damage parameter coupled to a critical-plane. This type of fatigue damage approach was adopted by Leidermark et al. [20], which was shown to be promising for predicting crack initiation under TMF conditions in the turbine rotor superalloy RR1000.

As the thermomechanical fatigue crack initiation life of gas turbine components is attributed by the accumulation of damage during the loading cycles, predictions using state of the art constitutive and fatigue models generate crack initiation lives based on the adopted parameters. These parameters are, usually, obtained by fitting appropriate models to describe the real material behaviour using optimisation procedures. Hence, generating a set of constitutive parameters that adequately describes the constitutive response and ditto for the fatigue behaviour. However, there exist no such thing as a perfect material, and scatter is always present in a material, due to *e.g.* imperfections or different material batches. Beretta et al. [21] showed that the cyclic stress–strain responses for 950X and 9CrMo steels exhibit significant scatter, where the same given load led to different fatigue lives that might correlate to the difference of microstructural growth processes ahead of the main crack tips. This can, for instance, be schematically shown by the fictitious "experimental" points in Fig. 1, where a significant scatter has been fictitiously reproduced for different loading conditions and fitted with an Ramberg–Osgood expression. It can clearly be seen, if these fictitious results were real responses, that different fatigue lives were obtained for the same applied load. The fitted Ramberg–Osgood curve describes the baseline response of the experimental data, however not capturing the outliers or their responses. Hence, the scatter in the real material behaviour needs to be accounted for, *i.e.* different constitutive parameter set-ups that include the effect of scatter (outliers), and by doing so the predicted fatigue crack initiation life will also be dependent on that scatter. Inclusion of scatter in material data has previously been studied, both with respect to probabilistic design and Monte-Carlo approaches concerning the fatigue life. Lehmayr and Staudacher [22] recommend Monte-Carlo "black-box" simulations for estimating the fatigue life of components, where $S-N$ curve parameters were exposed to statistical distribution to account for scatter in the material data to obtain scatter in the fatigue life. Crack initiation modelling in the turbine disc superalloy IN718 was conducted by Deyber et al. [23] by use of probabilistic methods. They proposed a global macroscopic and probabilistic model used in a post-process procedure to account for low-cycle fatigue scatter by means of observed micro-mechanisms. Musinski and McDowell [24] developed a microstructure-sensitive model coupling microstructural heterogeneities to size effects and fatigue scatter in a polycrystalline nickel-base superalloy undergoing high-cycle fatigue loadings. They showed by cumulative distribution function (CDF) and probabilistic strain-life that larger notch sizes yields a larger notch size effect and fatigue knock-down effect, giving improved high-cycle fatigue crack initiation prediction possibilities. The influence of combining stochastic analysis of material variability, load fluctuations and cyclic constitutive parameters on the multiaxial low-cycle fatigue assessment of notched steel components using a probabilistic framework was established by Zhu et al. [25]. For more recent work in fatigue reliability assessment of turbine disk with emphasis on multi-source uncertainties, such as material variability, load variation and geometrical uncertainty, please see Zhu et al. [26], Zhu et al. [27] and Niu et al. [28]. Instead of introducing scatter on the material parameters Leidermark et al. [29] evaluated the effect of scatter on the fatigue crack initiation life of a coarse-grained nickel-base superalloy by applying a crystal-plasticity constitutive model for each grain and introducing scatter with regard to grain orientation and location in comparison to a notch by using a Monte-Carlo analysis.

The aim of this paper is to investigate and quantify the effect of 'scatter in' on the constitutive parameters to the obtained 'scatter out' on the predicted fatigue crack initiation life by use of a simplistic and industrially affordable concept of the aerospace gas turbine rotor superalloy RR1000. An FE-model using an appropriate material behaviour description is subjected to an engine relevant load cycle of out-of-phase TMF type, containing different aspects of a flight cycle. A TMF crack initiation model based on fatigue damage accumulation using the memory surface concept is adopted. The scatter in the obtained fatigue crack initiation life is evaluated by performing a Monte-Carlo analysis of the FE-model, where scatter is introduced in the constitutive model using correction factors, obtained by singular value decomposition (SVD), on the used constitutive parameters with respect to baseline (mean) parameter values. It is to be noted that no experimental comparison to the obtained fatigue lives is done in this work, as the focus lies on evaluating the obtained scatter of the fatigue lives based on the scatter in the constitutive parameters while holding the fatigue parameters constant in the employed crack initiation model. This is of high relevance to the industry, since gathered material responses from previous experimental campaigns can be incorporated with new ones to asses the validity of both constitutive parameters as well as predicted fatigue lives.

2. Constitutive behaviour

As the aim of this paper is to quantify the effect of scatter in constitutive parameters to the obtained scatter in the predicted fatigue crack initiation life, the material data and response of the coarse-grained version of the powder-processed γ'-strengthened polycrystalline nickel-base superalloy RR1000 has been investigated, see *e.g.* Engel et al. [30]. The constitutive behaviour and the TMF crack initiation life, using a fatigue damage accumulation model, under a flight representative load cycle of this material has previously been modelled with success, see Leidermark et al. [20]. The corresponding constitutive model has herein also been utilised to describe the elastic and inelastic constitutive behaviour under the specific load condition consisting of a rate dependent Perzyna viscoplastic material description [31], and was implemented as a user-defined material subroutine in an FE-context. This constitutive model is able to describe the cyclic evolution of the material by two non-linear Armstrong-Frederick back-stress terms [32] (and also reproduced in [33]) and a saturated isotropic hardening term. In what follows, all tensors are presented in symbolic notation, where second-order tensors are quantified by upper-case Roman or Greek-letters and scalar valued parameters are defined by lower-case Roman and Greek-letters, restricted to a single Cartesian coordinate system. Furthermore, functional arguments are given in closed bracket form, *e.g.* the function h with argument $x, h = h[x]$.

The total strain tensor can be decomposed into an elastic and an inelastic strain

$$\boldsymbol{\varepsilon} = \boldsymbol{\varepsilon}^{e} + \boldsymbol{\varepsilon}^{in} \tag{1}$$

where the elastic response is obtained by Hooke's law, using the elastic stiffness tensor $\mathbb{C}^{e}_{ijkl}$ with an isotropic material description based on the Young's modulus E and Poisson's ratio.

The following yield function was employed

$$f = \sigma^{vM}_{eq}[\widehat{\boldsymbol{\sigma}} - \boldsymbol{B}] - r - \sigma_Y \tag{2}$$

where $\widehat{\boldsymbol{\sigma}}$ denotes the deviatoric stress tensor, $\boldsymbol{B}$ is the total back-stress tensor, r is the isotropic hardening term, σ_Y is the initial yield limit and σ^{vM}_{eq} is the von Mises equivalent stress, defined as

$$\sigma^{vM}_{eq} = \sqrt{\frac{3}{2}(\widehat{\boldsymbol{\sigma}} - \boldsymbol{B}) : (\widehat{\boldsymbol{\sigma}} - \boldsymbol{B})} \tag{3}$$

The total back-stress term is based on additive decomposition [34] of the two individual back-stress terms, $\boldsymbol{B} = \sum_{k=1}^{2} \boldsymbol{B}_k$, where the evolution law for each term is defined by

$$\dot{\boldsymbol{B}}_k = c_k\left(\frac{2}{3}a_k\dot{\boldsymbol{\varepsilon}}^{in} - \boldsymbol{B}_k\dot{\lambda}\right) \tag{4}$$

with the individual hardening parameters c_k and a_k.

To describe the cyclic softening of the stress state typically seen in these materials, a non-linear isotropic hardening term has been adopted, where the evolution law is given by

$$\dot{r} = h(q - r)\dot{\lambda} \tag{5}$$

where h describes the rate of cyclic softening and q the saturation.

The evolution law of the inelastic strain tensor is defined by the Perzyna flow rule based on the adopted yield function as

$$\dot{\boldsymbol{\varepsilon}}^{in} = \begin{cases} 0, & f \leqslant 0 \\ \dot{\lambda}\dfrac{\partial f}{\partial \boldsymbol{\sigma}}, & f > 0 \end{cases} \tag{6}$$

in which the inelastic multiplier is defined by the following power-law relation, *cf.* Odqvist [35]

$$\dot{\lambda} = \left(\frac{f}{\eta}\right)^{m} \tag{7}$$

where m and η are constitutive parameters accounting for the viscous effects.

The discretisation of the internal stress update routine was defined using a Newton–Raphson iterative procedure, *cf.* Ottosen and Ristinmaa [36], where, explicitly, the inverse of the Jacobian matrix is needed to calculate the unknowns, which are obtained by the iterative procedure during the inelastic corrector step when $f \to 0$. Additionally, the evolution laws of the back-stress terms and the non-linear isotropic hardening term, the recovery term of these are usually discretised by use of the previous state. However, instead of using the value of the previous state, the current state's value has been applied by introducing a correction term, as shown by Kobayashi and Ohno [37], by updating the correction term in the internal Newton–Raphson stress update routine, hence by adopting a radial return approach for the back-stresses and isotropic hardening. This offers a better representation of the actual response at state $n+1$ for relative large time steps, but the difference decreases with decreasing time step size.

A database of 70 isothermal material tests was utilised in the present work to approximate the scatter in the constitutive parameters. All tests may be termed "cyclic inelasticity" tests, meaning that an appreciable amount of inelastic strain is accumulated in each loading cycle. Microstructural damage is a result of reduced load-carrying capability and is here defined as loss of stiffness, as per traditional continuum damage mechanics *cf.* Lemaitre and Sermage [14], therefore the onset of damage accumulation can be approximated in cyclic inelasticity hysteresis loops by monitoring the apparent Young's modulus (from the elastic regime) between loading cycles and noting when the value begins to monotonically reduce following stabilised behaviour. Damage is not incorporated into the hardening model discuss here, therefore only hysteresis loops prior to this damage onset point are considered in constitutive parameter determination activities. All data sets are uniaxial in nature and are strain controlled. Furthermore, loading strain rates are consistent between experiments. In short, only test temperatures, peak loads and loading ratios are modified between the experimental data sets. Resource material for all specimens was taken from component forgings and, at least in an industrial context, may be regarded as consistent. It is

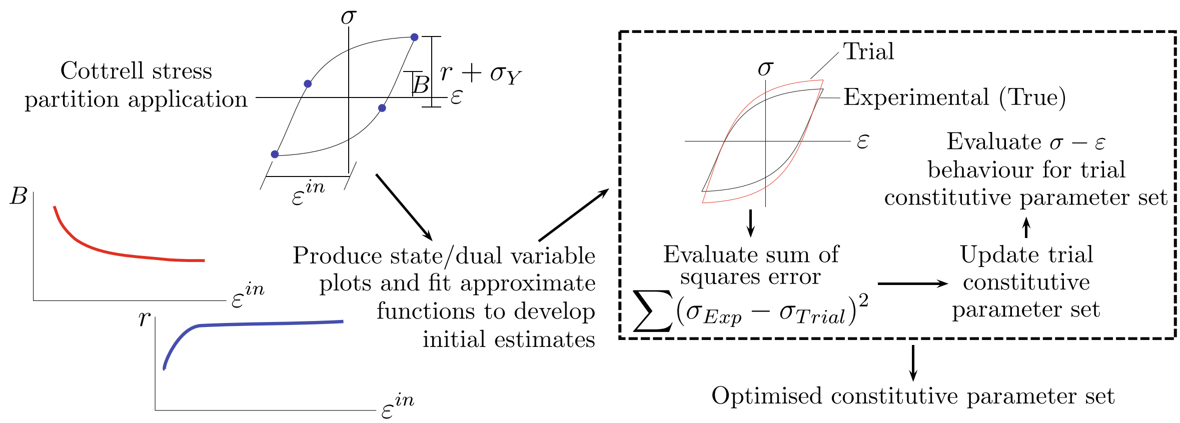

Fig. 2. Schematic flowchart of constitutive parameter fitting procedure.

of course true that different parts of a forging will experience different thermal histories due to varying section thickness in the component and tooling, thereby giving potential for spatially dependent material characteristics. In practice these variations are often not adequately traced however, therefore the specimens are regarded as identical. It is important to note here that any of the 70 experimental data sets may be used to determine values for material dependent parameters at the given test temperature. In the present work, interest is focused on scatter in the constitutive parameters. One may ask questions such as “How sensitive are crack initiation life estimates to constitutive parameters?” or “What would have happened if I had calibrated my hardening model using this test data over that test data?”. The present work attempts at answer these questions.

Constitutive parameters for the above presented constitutive model were acquired by an optimisation procedure of the 70 isothermal experiments across the temperature range from a material database of performed experiments on RR1000. For the sake of brevity a schematic representation of the constitutive parameter fitting procedure can be seen in Fig. 2, however it should be noted that it is based on Cottrell’s stress partitioning method [38], which uses a linear regression approach to determine the onset of inelasticity, and may be found in for instance [39–41]. Following the determination of constitutive parameter estimates an optimisation procedure was implemented in order to “fine tune” values. Simple objective functions based on the difference between experimental and predicted (using a trial constitutive parameter set) stress magnitudes were utilised in Matlab’s LSQNONLIN function (the well known solver ODE45 was used to solve the differential equations outlines above). Although the phenomenological constitutive parameters defined above are not “fundamental” in a way, the stress partitioning approach used here provides a consistent parameter determination approach. The present work assumes that this consistency allows for sampling to be conducted along linearly independent projections of the data set. This will be achieved using the eigenstructure of singular value decomposition to perform principal component analysis (PCA) [42].

The constitutive parameters defined in the model outlined above are temperature dependent. For a given collection of isothermally determined constitutive parameters it is convenient to fit a continuous function such that parameter interpolation can be conducted for intermediate temperatures in, say, a flight representative TMF cycle see *e.g.* [41]. This can easily be accomplished using general exponential functions (for example, EXP2 in Matlab) such that some asymptotic behaviour is achieved. In the present work, scatter in constitutive parameters is introduced through a series of correction factors (later designated by k_α) which modify the baseline (mean) temperature dependent constitutive parameter functions. Values of correction factors are sampled from distributions that are developed from constitutive parameter. That is to say, for a particular constitutive parameter (i.e. one of the ten defined above), 70 constitutive parameter values are determined from the database of 70 isothermal tests. The arithmetic mean of each of these constitutive parameters at each isothermal test temperature is then calculated and each constitutive parameter value is expressed as a factor of it, i.e. a particular constitutive parameter value at a given temperature is expressed as a factor of the mean constitutive parameter value for that temperature. The database of 70 isothermal tests therefore generate 10 distributions which describe the variance of each material. In effect, the process outlined in the present work samples correction factors from each of these distributions (or, more accurately, from the PCA distributions developed from them) and then applies it to the associated temperature dependent constitutive parameter function. The temperature dependent constitutive parameter function are themselves defined by the temperature-wise mean values. The correction factors therefore act to modify a baseline temperature dependent set of constitutive parameters. It should be noted that discrete testing temperatures were used to produce the database of 70 isothermal tests used in the present work. Test temperatures are evenly spaced over the temperature range relevant to most aero-engine turbine disc and rotor components, and equal numbers of tests are used for each discrete temperature. In this way bias for a particular test temperature is avoided. The correction factor sampling approach clearly assumes that variance in constitutive parameters manifests independent of temperature. Distributions in correction factors for each constitutive parameter are given in Fig. 3, along with temperature separated means and standard deviations. The limited amount of data (70 tests) available and the lack of a clear trend between test temperature and correction factor scatter has prompted the assumption that constitutive parameter scatter is independent of temperature in the present work. Analysis of correction factor distributions did not highlight any trend between variance and test temperature (thereby supporting this assumption), however this should be explored in future work through analysis of broader data sets.

3. Fatigue damage accumulation model

Crack initiation is mainly a surface dominant phenomena, and hence the fatigue damage accumulated at the surface has to be evaluated. Based on this, the fatigue damage accumulation model developed in Leidermark et al. [20] was adopted herein to evaluate the crack initiation life of the investigated aerospace rotor superalloy. The model is based on the memory surface concept, see *e.g.* Jiang [19], and consist of a fatigue damage term ω that incorporates the material memory and inelastic strain energy ψ^{in} in the point of interest, hence eliminating the need of a cycle-counting method. The fatigue damage accumulation model consists of the following memory surface function

$$g = \sqrt{\hat{\boldsymbol{\sigma}} : \hat{\boldsymbol{\sigma}} - \sqrt{\frac{2}{3}}\sigma_{mem}} \tag{8}$$

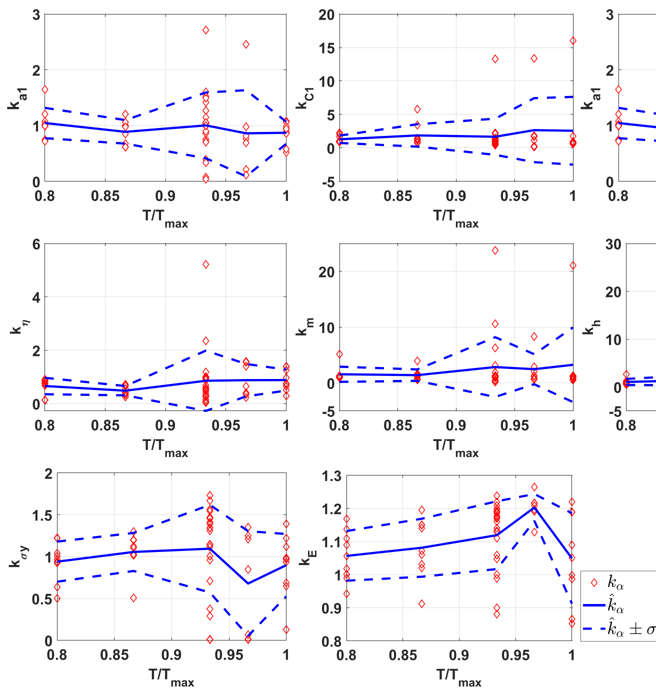

Fig. 3. Distributions of correction factor for each constitutive parameter over the analysed temperature range. It is to be noted that k_α represents the correction factor, $\widehat{k}_\alpha$ is the mean value and σ is the standard deviation of the corresponding constitutive parameter α.

which is based on the memory stress σ_{mem} and the current deviatoric stress state. The memory stress is initially set to be equal to the fatigue endurance limit σ_{end} and fatigue damage is only developed if $g = 0$. The original set-up of the evolution of the memory stress is defined as

$$\dot{\sigma}_{mem} = \sqrt{\frac{3}{2}}\mathscr{H}[g]\left\langle \frac{\widehat{\boldsymbol{\sigma}} : \dot{\widehat{\boldsymbol{\sigma}}}}{\sqrt{\widehat{\boldsymbol{\sigma}} : \widehat{\boldsymbol{\sigma}}}} \right\rangle - \beta(1 - \mathscr{H}[g])(\sigma_{mem} - \sigma_{end})\dot{\lambda} \tag{9}$$

where the Heaviside function $\mathscr{H}[g]$ makes sure that the memory surface contracts when the stress state is lower than the memory stress ($g < 0$) and expands when it is on the memory surface ($g = 0$). In the original expression of the memory surface evolution, the parameter β defines how much the surface contracts when the loading is changed from a high to a lower amplitude loading. However, the applied flight representative load cycle used in this study consists of constant amplitude loading, meaning that no contraction will occur, and as a consequence a simplification can be made to cancel the contraction capability by setting β equal to zero in Eq. (9).

The fatigue damage accumulation is based on the inelastic strain energy measure ψ^{in} and the damage evolution is as follows

$$\dot{\omega} = \langle \sigma_{mem} - \sigma_{end} \rangle^{\alpha} \dot{\psi}^{in} \tag{10}$$

here, α is a fitting parameter and damage accumulation is directly coupled to the memory surface using the memory stress to account for load-sequence effects.

A simplistic multiaxial approach for the inelastic strain energy evolution was adopted based on inspiration by the work by Ostergren [8]. This model assumes that fatigue damage is accumulated in all increments during tensile loading by pairing the equivalent von Mises stress with the magnitude of the instantaneous inelastic strain rate during the actual load increment. Thus, the following inelastic strain energy evolution was considered in this work

$$\dot{\psi}^{in} = \mathscr{H}[\mathrm{tr}\boldsymbol{\sigma}]\sigma_{eq}^{vM}\dot{\lambda} \tag{11}$$

Hence, accounting for the tensile loading by use of the Heaviside function on the trace of the stress tensor.

The fatigue damage model was included in the above described user-defined material subroutine as a stand-alone subroutine with inputs directly from the constitutive model. It is worth mentioning, that this implementation of the fatigue damage model is not coupled to the stress update in the constitutive model, as traditionally done for continuum damage models. As the fatigue damage is updated incrementally during each time step the stress and strain state in each increment is directly fed into the fatigue damage subroutine, and by this, the history of the fatigue damage is accounted for and evolves in subsequent iterations until the critical damage is reached, initiating a macroscopic crack. Consequently, the incremental damage accumulated from the load steps are summed up over the entire loading sequence to the critical value ω_c. The number of cycles to crack initiation can be evaluated based on the damage accumulated during each fully undergone load cycle, as

$$\sum_{i=1}^{N_i} \Delta\omega_i = \omega_c \tag{12}$$

where $\Delta\omega_i$ is the amount of accumulated damage in one loading cycle and N_i is the number of cycles until crack initiation. This equation can be simplified, as the global stress state in nickel-base superalloys usually stabilises after a couple of cycles, into the following

$$\omega_c = \omega_1 + \cdots + \omega_{stable}(N_i - N_{stable}) \tag{13}$$

where a stable state is reached after N_{stable} number of cycles. Hence, taking advantaged over the fact that the fatigue damage evolution will also stabilise. This saves the number of performed cycles, as it is too computational expensive to run all cycles up to crack initiation, which nominally ranges from, depending on load level, 100 –10000 cycles in TMF loading applications, see *e.g.* Lancaster et al. [43] or Wang et al. [44]. An approach to actually simulate all cycles could be to use a cycle jumping procedure, to speed-up the computational effort, see *e.g.* Leidermark and Simonsson [45]. This has not been done here, as Eq. (13) offers an adequate compromise. A stable damage state was, in this work, defined by a moving average value of three states where the decrease was less then 5%. More details about the fatigue damage model and the acquisition of the fatigue damage parameters (σ_{end}, α and ω_c) can be found in Leidermark et al. [20].

4. Evaluation

Based on the fact that the constitutive behaviour of the material drives the response of any loaded structure, and also the obtained fatigue life, only the scatter in constitutive parameters have been considered in this work. This is in line with that a variation in inelastic strain range, which typically is involved in driving the damage in a material and hence fatigue life, is directly coupled to the used inelastic constitutive parameters in a constitutive description. Hence, to evaluate the effect of the scatter in constitutive parameters of the constitutive model, a correction factor was defined for each constitutive parameter present in the adopted constitutive model. In this case, ten correction factors were defined in total, denoted by k_α. The fatigue damage parameters were not exposed to any scatter, and the values obtained in Leidermark et al. [20] were used for all simulations, as the effect of scatter was only to be evaluated with respect to the constitutive parameters. To maintain a physical representation of the constitutive parameters and the respective response in correlation to the generated correction factors, an SVD was performed to generate a basis for the factors. This was then fed into a Monte-Carlo analysis to evaluate the fatigue crack initiation lives over the entire spectrum of possible correction factors.

4.1. Singular value decomposition

The effect of variance in constitutive parameter values on predicted fatigue life may be explored through Monte-Carlo type analyses, wherein trial sets of constitutive parameters are generated by sampling from set of distributions before analyses are conducted. This process allows deviations from some baseline to be quantified. Sampling of constitutive parameters from said statistical distributions must be done with care however as it is almost certain that there will exist some level of correlation between constitutive parameter variations (*i.e.* constitutive parameter co-variance matrices will almost certainly not be diagonal). It would be expected, for example, that the kinematic hardening parameters (c_1, a_1, c_2, and a_2) will show a high level of correlation as they relate to a single phenomenological behaviour. If constitutive parameters do not vary independently it is not permissible to sample from their respective distributions independently. In the present work, PCA is used to determine independent projections of the constitutive parameters such that sampling may be made conveniently. PCA looks to determine weighted linear functions of co-variant parameters (here the constitutive parameters) such that the projections on to these principal components are independent (*i.e.* co-variance matrices of the constitutive parameters projected into the principal component space are diagonal). It is important to note that, in order to describe all variance in the data, as many principal components as there are variables are required. PCA is often used as a method of order reduction, but this utilises the fact that some PCA components will account for less variance, i.e. it possesses a smaller corresponding singular value. In the present work all PCAs are used to make the transformation between original variables and the PCA projections more convenient. PCA assumes a linear mapping and structure to the data. This assumption is not explored in the present work, however future efforts (with larger data sets) may look to test this assumption by comparison PCA results to alternatives such as locally linear embedding. In practice, PCA may be readily conducted by noting the eigenstructure of SVD matrices. SVD can be summarised by the following equation

$$\boldsymbol{X} = \boldsymbol{U}\boldsymbol{S}\boldsymbol{V}^T \tag{14}$$

wherein the (possibly non-square) matrix $\boldsymbol{X}$ is decomposed into the matrices $\boldsymbol{U}, \boldsymbol{S}$, and $\boldsymbol{V}$. Note that, in the present work, $\boldsymbol{X}$ is the matrix of all observations of $k_\alpha^{'}$ (defined later in this section). Intuitively, the matrices $\boldsymbol{U}$ and $\boldsymbol{V}$ can be seen as rotations and $\boldsymbol{S}$ can be seen as at set of "scalings" applied after the application of the rotation defined by $\boldsymbol{V}$. It can be shown that, for centred sets of variables, the rows of $\boldsymbol{V}^T$ are the weightings required for PCA. The orthogonal matrix $\boldsymbol{V}$ therefore allows for the projection of the variables into the principal component space. This method has been applied in the present work, where in the interest of clarity, the constitutive parameters used in the present work are E (Young's modulus), σ_Y (yield limit), c_1, a_1, c_2, and a_2 (relating to kinematic hardening), h and q (relating to isotropic hardening), and m and η (relating to inelastic flow). The only one excluded was the Poisson's ratio, present in the elastic stiffness tensor, as only uniaxial tests were used in the parameter identification process and no measurements of contractions were available in the material database. Thus, no variation of this parameter could be physically defined.

Typical constitutive parameter variations must be approximated before any kind of sampling can be made. Baseline values for the constitutive parameters used in the present work were determined by defining functions with temperature arguments. These functions describe how individual constitutive parameters vary with temperature and represent a nominal, or mean, material response. Variations in constitutive parameters are explored here by multiplying each parameter by a corresponding correction factor, denoted by k_α, where α corresponds to the relevant constitutive parameter. Variations in constitutive parameters are determined by performing optimisation operations on k_α values, such that modified constitutive parameters (baseline constitutive parameters multiplied by corresponding k_α values) describe experimentally observed isothermal cyclic responses. A range of temperatures, load ranges, and load ratios were used in k_α optimisation procedures. In the present work, 70 sets of k_α values have been determined using this method, due to the amount of accessible experimental data. No correlation was observed between temperature/loading rate/loading ration and k_α here, suggesting that all k_α data may be used to fit distributions and generated k_α values (used in subsequent Monte-Carlo analysis) may be applied to all loading conditions and temperatures. In all optimisation procedures, initial conditions of unity were applied to all k_α. Furthermore, the variables must be centred in order for SVD to be used for PCA. Hence, each k_α was therefore decomposed in accordance with

$$k_\alpha = \widehat{k}_\alpha + k_\alpha^{'} \tag{15}$$

where $\widehat{k}_\alpha$ is the mean of k_α (across all observations) and $k_\alpha^{'}$ is an observation specific deviation from the mean. Note that k_α and $\widehat{k}_\alpha$ must be positive (in order to preserve the sign of the constitutive parameters to which they relate), whereas $k_\alpha^{'}$ can be either positive or negative. After centring variables, only distributions in $k_\alpha^{'}$ are relevant. In all cases in the present work, t-scale distributions were fitted to data in order to evaluate probability density functions (PDFs). PDFs may then be summed in order to generate CDFs. It is then a trivial matter to sample from the original distribution, based on an input variable (here denoted as ζ) in the closed interval of $[0,1]$ to interpolate a parameter value from the CDF, see Fig. 4 for a schematic representation of this sampling. The PDF of the t location-scale distribution can be expressed by

$$p[x] = \frac{\Gamma\left[\frac{\nu+1}{2}\right]}{p\sqrt{\nu\pi}\Gamma\left[\frac{\nu}{2}\right]}\left(1+\frac{1}{\nu}\left(\frac{x-\mu}{p}\right)^2\right)^{-\frac{\nu+1}{2}} \tag{16}$$

where $\Gamma[]$ is the gamma function, p is a scaling parameter, μ is a location parameter, and ν is a shape parameter. In the present work, PDFs and CDFs are determined using Mathworks statistical toolbox, implemented through Matlab [46]. For illustrative purposes, distributions of $k_\alpha^{'}$ are shown in Fig. 5. Note that, for the reasons outlined above, $k_\alpha^{'}$ values may

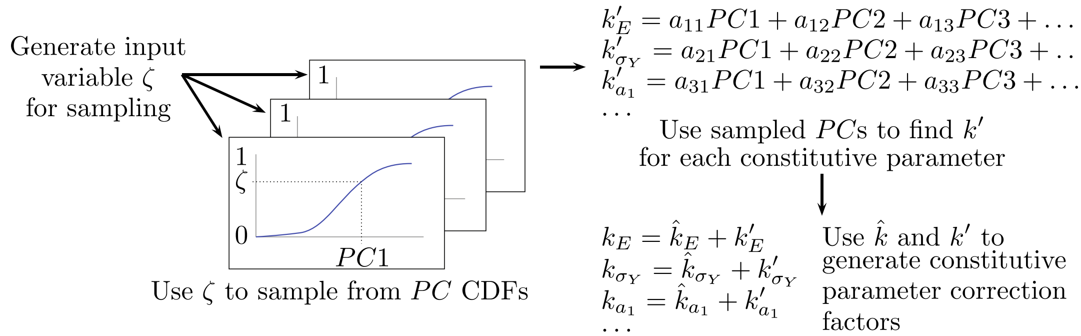

Fig. 4. Schematic flowchart of the CDF sampling.

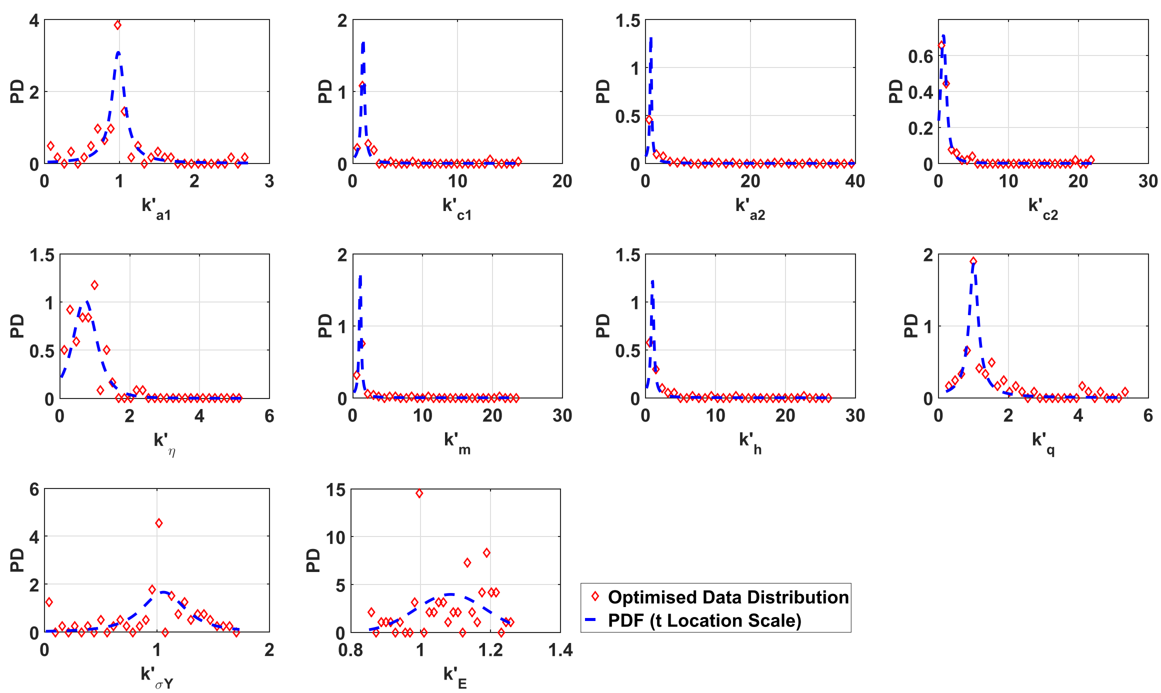

Fig. 5. Statistical distributions (t location-scale fitted) of correction factor deviations ($k_\alpha^{'}$). (PD: probability density).

not be sampled directly from these. SVD has been conducted on the observation matrix of $k_\alpha^{'}$ in order to determine principal components ($PC1$-$PC10$) and distributions determined for each principal component projection, as shown in Fig. 6. From PDF functions CDFs may be determined, as shown in Fig. 7. When a set of k_α values was to be generated, principal component values were first sampled from CDFs (by using the input variable ζ confined to the closed interval of $[0, 1]$ and interpolating the CDF). Principal components may then be project back into $k_\alpha^{'}$ space (using the inverse of $\boldsymbol{V}$ in Eq. (14)), with k_α values determined by adjusting $k_\alpha^{'}$ in line with Eq. (15). Note that the inversion of $\boldsymbol{V}$ is not usually expensive as its dimensions are small and equal to the number of variables considered, ten in this work.

4.2. Monte-Carlo analysis

A Monte-Carlo analysis with Latin Hypercube sampling based on a uniform distribution for the input variable ζ was performed in LS-OPT, version 5.1.1 [47]. The uniform distribution confined to the closed interval of $[0, 1]$ was restricted to the interval of $[0.1676, 0.8691]$, due to that values outside this interval generated negative correction factors with the adopted CDF, which is not an option. One hundred FE-simulations were performed, each with a unique set of correction factors, with the implicit solver in LS-DYNA, version R7.0 [48]. The FE-model consisted of a cube containing one eight-noded brick element, with reduced integration, which was loaded with twelve subsequent flight representative load cycles. The flight representative load cycle is an out-of-phase strain-controlled TMF load cycle, containing different aspects of a flight cycle, such as take-off, climb, cruise and decent, and is schematically depicted in Fig. 8. The choice of load cycle is connected to what a relevant component in the hot section of the gas turbine will experience. With the combination of the hot gas and mechanical load the hottest part in a critical component will experience a so called “hot-spot”, mainly due to insufficient cooling capabilities, which is attributed by its higher temperature with respect to its surroundings. The “hot-spot” wants to expand but is restricted by the surroundings, which leads to large compressive stresses, hence out-of-phase TMF load conditions, see *e.g.* Moverare et al. [49]. Furthermore, the presented flight cycle was used in the experimental investigation of RR1000 by Messe et al. [50] and also in the previous characterisation and calibration work of the fatigue damage model by Leidermark et al. [20], where the fatigue endurance limit was coupled to this specific load cycle. However, in this study the applied strain range in all simulations was 0.9061%. The above presented user-defined material model with inclusion of the fatigue damage accumulation model was utilised to evaluate the

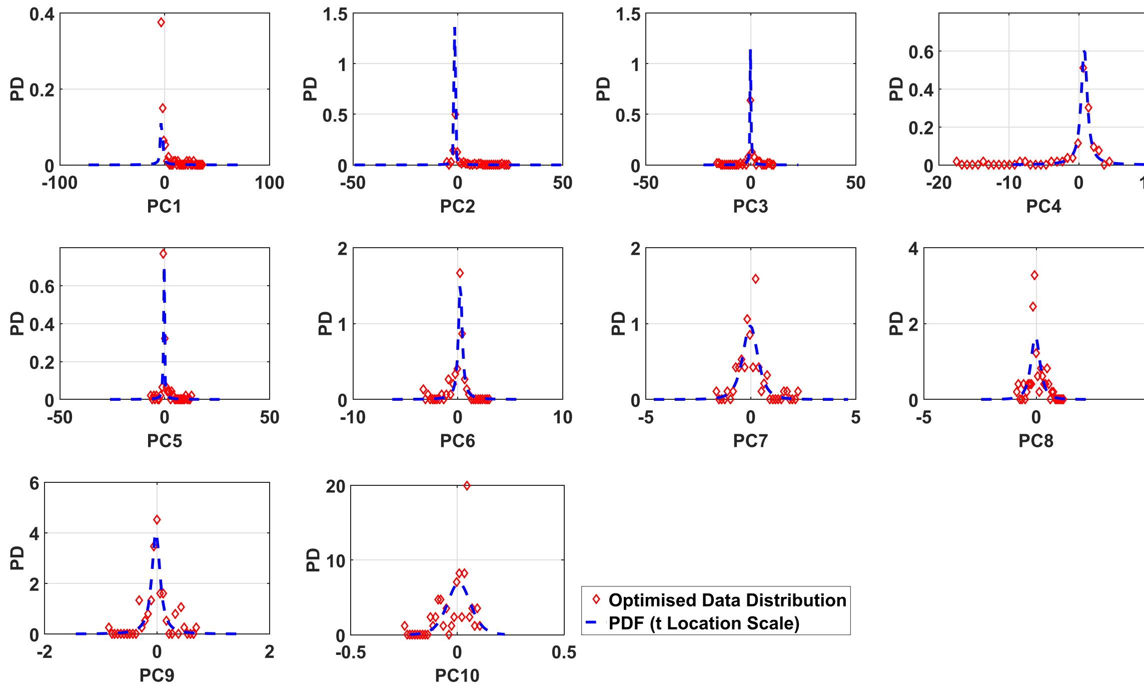

Fig. 6. Statistical distributions (t location-scale fitted) of principal component projections ($PC1$-$PC10$) of correction factor deviations ($k_{\alpha}^{'}$). (PD: probability density).

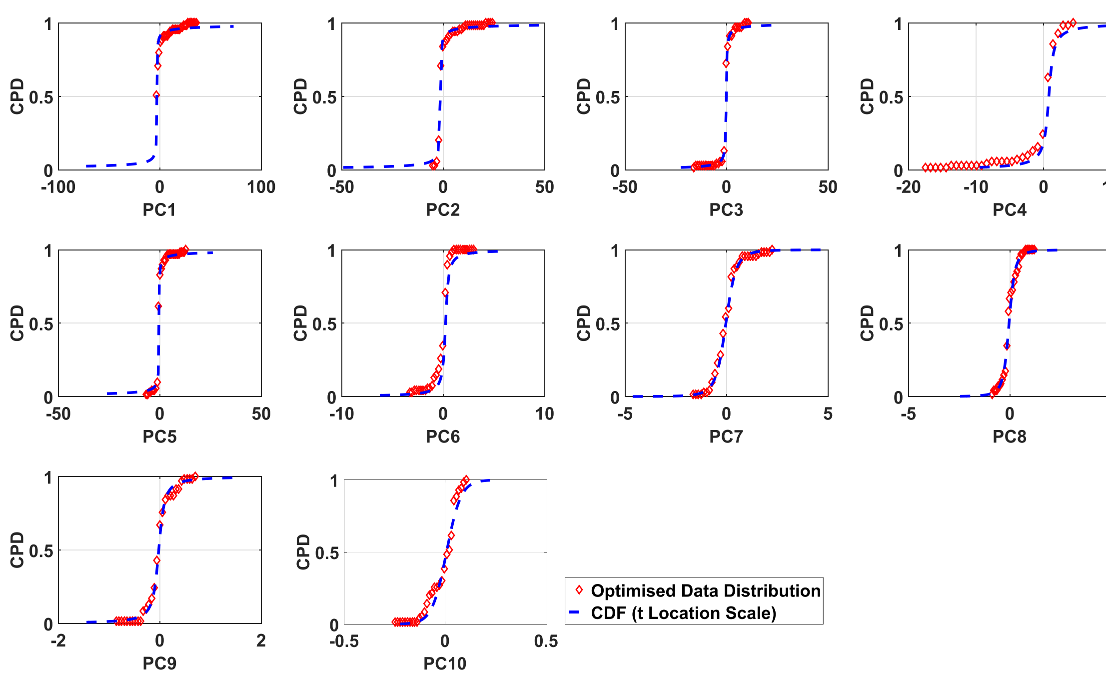

Fig. 7. CDF fits (based on t location-scale distributions) of principal component projections ($PC1$-$PC10$) of correction factor deviations ($k_{\alpha}^{'}$). (CPD: cumulative probability density).

stress–strain response as well as the fatigue crack initiation life. For comparative reasons an FE-analysis with all correction factors set to unity was also performed, with the same set-up otherwise, to obtain the fatigue crack initiation life for the baseline constitutive parameters. The work flow in the Monte-Carlo analysis can be observed in Fig. 9, where it can be seen that LS-OPT was used to generate the input to the SVD and gather the resulting fatigue crack initiation lives for comparisons. Furthermore, note that no experiments were performed to be compared to, only dry-simulations were done to see the effect of scatter in constitutive parameters on the fatigue crack initiation lives. Worth to mention, is that the elapsed computational time (CPU time) for each FE-simulation was approximately 24s and they were performed in sets of 32 in the Monte-Carlo analysis, hence $32 + 32 + 32 + 4$, on a Linux-based cluster equipped with four Intel® Xeon® CPU E5 -2650 v2 @ 2.60GHz eight-core processors. One core was appointed per FE-analysis and the total time of completing the Monte-Carlo analysis took roughly 20 min.

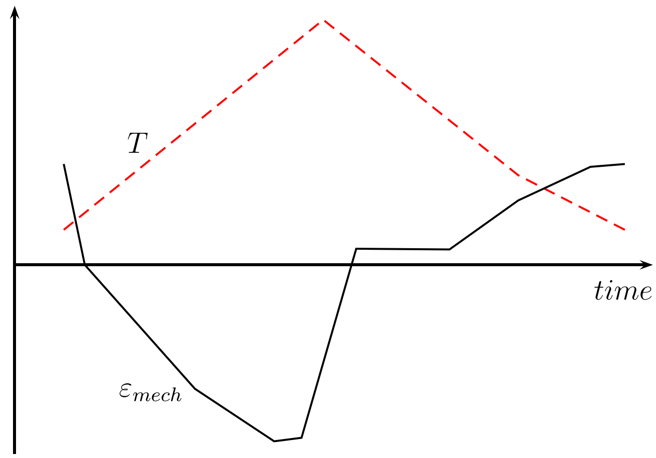

Fig. 8. Schematic representation of the applied flight representative out-of-phase TMF load cycle.

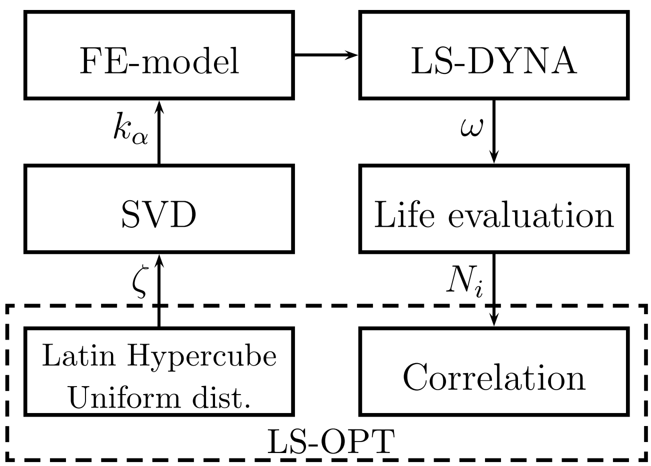

Fig. 9. Work flow of the Monte-Carlo analysis.

5. Results and discussion

From the performed Monte-Carlo analysis, with the adopted material model and fatigue damage model, the obtained fatigue crack initiation lives in comparison to the input variables to the SVD (correction factors) can be seen in Fig. 10. It is to be noted that the predicted lives have been normalised with the crack initiation life obtained from the simulation using the baseline constitutive parameters, hence a normalised fatigue crack initiation life of unity in the figure corresponds to that of the baseline simulation. From this it can be observed that 42 set of correction factors gave infinite fatigue lives, illustrated by a life of zero in the plot, as the endurance limit was never reached in the damage accumulation model or that no inelastic flow was present during tensile loading. It can also be visualised in the plot that the predicted fatigue crack initiation lives are localised and display a low scatter compared to the input scatter into the constitutive model, as in the interval of $0.348 < \zeta < 0.655$ the baseline life is more or less obtained, where the square root error estimate is 0.2571. Furthermore, it can be seen in the figure that values larger than 0.655 of the input variable predict increasing lives, which are very high compared to baseline. These points are related to the fact that the correction factor for the yield limit is increasing, *cf.* Fig. 11, which generates responses with a more elastic dominant state, where damage is introduced later in the cyclic loading and eventually an elastic response ($\zeta > 0.753$) during the tensile part of the hysteresis will be present. It can also be observed that for values lower than 0.348 zero (infinite) lives are obtained, and the reason for this is that at these levels the generated correction factor of the yield limit is decreasing with decreasing ζ, *cf.* Fig. 11, and thus viscoplasticity is introduced at lower and lower stress states and not enough memory stress is accumulated to overcome the endurance limit in Eq. (10), giving no fatigue damage accumulation.

The number of cycles to a stable damage state is also represented in Fig. 10, where for non-run-outs the stable state is increasing with increasing input variable value, also showing the tendency of a more elastic dominant tensile response as damage is introduced later. For certain input variables ($\zeta > 0.655$) the set of correction factors generated damage, but the stable damage state with a difference of 5% was not reached. To accommodate for this, the mean value of the last three damage values, trailing back from the completed twelfth cycle, was defined to reach the stable state, even thou it did not. This is of course not an entirely correct approach, but with the retrospective that all previous values of the input variable generated stable damage states and that the memory surface at these levels did not evolve any further, it can

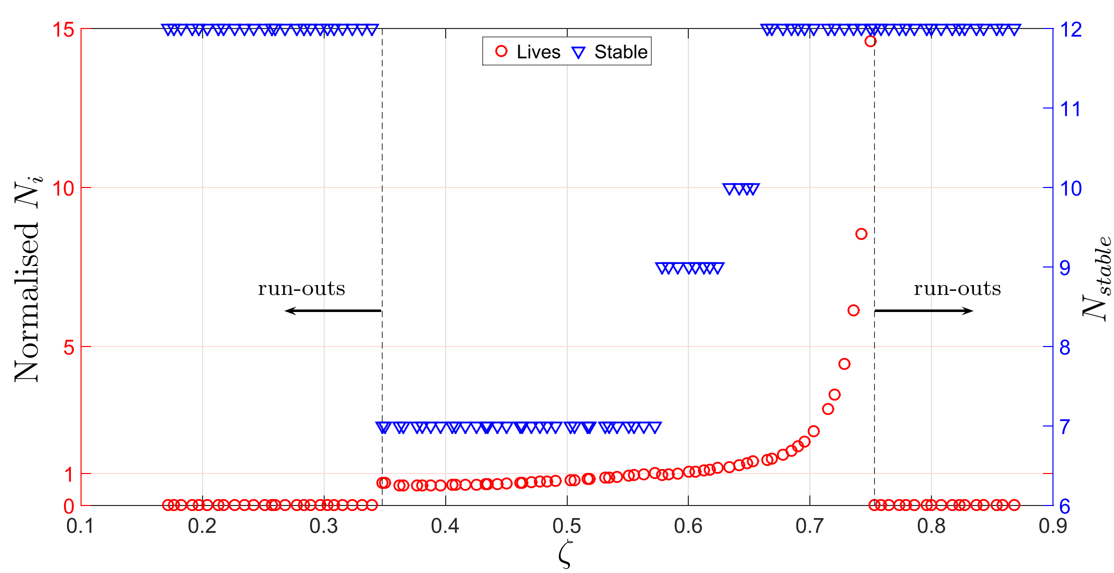

Fig. 10. Normalised fatigue crack initiation lives and the number of cycles to the stable state versus the input variable.

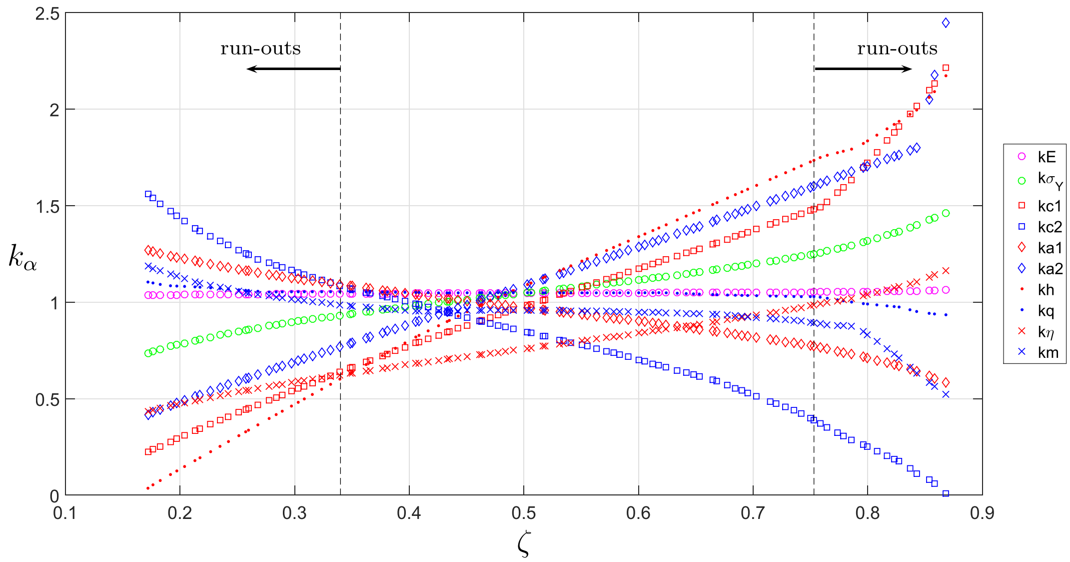

Fig. 11. Corrections factors versus the input variable.

be seen as a sufficiently good approach. No fatigue damage was generated for the run-outs, indicating infinite lives, however, this was represented by zero normalised fatigue crack initiation lives in Fig. 10 due to simplicity, and the corresponding stable state value was taken as the last (twelfth) cycle due to the above issue where the damage is introduced later and later in the cyclic loading.

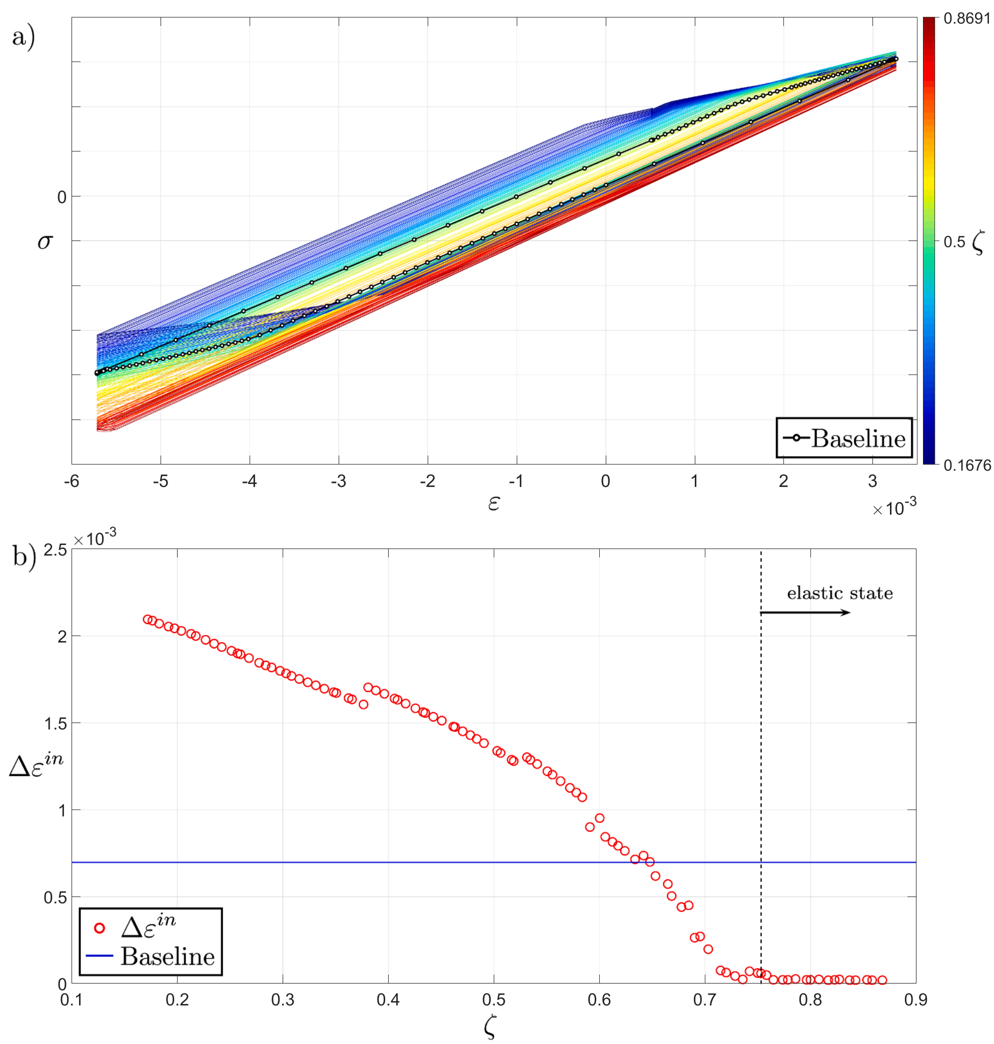

Fig. 12. The a) hysteresis loops and b) inelastic strain ranges at the stable damage state for all ζ values and the baseline constitutive parameters.

Regarding the run-outs, the hysteresis loop of all conducted simulations were plotted in Fig. 12a) at the stable damage state. It can be observed that a more elastic state is received for increasing values of the input parameter. This is also visible in Fig. 12b), which displays decreasing inelastic strain range at the stable damage state with increasing input variable. Run-outs are received for $\zeta > 0.753$, cf. Fig. 10, however at the twelfth loading cycle, which here have been deemed the last one in the extraction process, a fully elastic state is not received for all these loops. Nevertheless, this is due to that the stable damage state is obtained later and later, going towards a fully elastic state eventually, and responses in this interval is considered to be elastic in this context, *i.e.* not generating damage.

Focusing attention on the fatigue crack initiation life behaviour in Fig. 13, indicating a positively skewed distribution function. Therefore, a suitable choice of distribution for N_i can be the log-normal, where the following PDF has be adopted in this work

$$d[x] = \frac{1}{x\overline{\sigma}\sqrt{2\pi}} e^{-\frac{(\ln x - \overline{\mu})^2}{2\overline{\sigma}^2}} \tag{17}$$

where $\overline{\mu}$ is the mean and $\overline{\sigma}$ is the standard deviation of the logarithmic values of entity x, here to be N_i. Hence, further enhancing the insight that the introduced scatter in constitutive parameters on the obtained fatigue crack initiation lives are low, as the distribution is located around the life of the baseline constitutive parameters. Note that only the simulations that predicted non-infinite lives have been accounted for in the distribution function.

The fatigue damage parameters were kept to the initial values throughout the entire Monte-Carlo analysis, and this gives a specific touch to the problem. As can be seen in Fig. 10 infinite lives are predicted for $\zeta < 0.348$ based on the decreasing correction factor for the yield limit, *cf.* Fig. 11. This might be avoided if the endurance limit is also affected by the said correction factor, as the endurance limit is a product of the material's yield limit. With this in mind, a second Monte-Carlo analysis was conducted with inclusion of the yield limit's correction factor on the endurance limit in the fatigue damage accumulation model. The obtained results can be found in Fig. 14, where it is seen that for low values of the input variable, previous consisting of run-outs, now generate damage and reach a stable state after $3-5$ cycles. Thus, generating fewer run-outs in total, 30 in this case, but as a consequence the error estimate using square root over the larger interval of $0.168 < \zeta < 0.584$ increases to 0.4517 with respect to baseline. In addition, it can also be seen that in the interval of $0.585 < \zeta < 0.684$ infinite lives are obtained, but still there is a tendency of a continuous curve connecting the non-run-outs. The reason for this is that the stress state does not have the capacity to exceed $\sqrt{2/3}\sigma_{mem}$, *cf.* Eq. (8), as the memory stress is initially set equal to the endurance limit which in turn increases in this interval due to the correction factor. This leads to that no evolution of the memory stress occurs, *cf.* Eq. (9), and hence no damage accumulation, see Eq. (10). The fitting parameter α could also be exposed to the scatter, but this was not considered in this work as it is a fitting parameter with direct correlation to experimental observations.

With respect to the obtained error estimate in the two above cases, which only visualised the error with respect to baseline life, a better measure for quantifying the estimates of the 'scatter out' in terms of the predicted crack initiation lives due to the 'scatter in', based on the constitutive parameters, was done for the above respective intervals of the input variable. Based on this, the coefficient of variation was determined for both of these cases, and compared to the respective value of the input variable intervals, by the following

$$c_v = \frac{\overline{\sigma}}{\overline{\mu}} \tag{18}$$

where the mean $\overline{\mu}$ and the standard deviation $\overline{\sigma}$ of the input variable and the predicted crack initiation life, respectively, were used. The estimates are gathered for comparison in Table 1, where it can be seen that the second case, using k_{σ_Y} also on the endurance limit, gave a smaller scatter compared to the first case with respect to the 'scatter in' of the constitutive parameters. Showing the opposite trend compared to the previous square root error estimate in correlation to the baseline life. Furthermore, it is to be pointed out that different intervals of the input variable are present in the first and the second case.

In both Figs. 10 and 14, run-outs are predicted for values higher than 0.753 of the input variable. This can be explained by the fact that k_h is increasing, increasing the rate of softening, when at the same time k_q is decreasing below unity, *cf.* Fig. 11. Thus, increasing the total response (hardening is obtained) of the isotropic hardening term, yielding an increase of the elastic regime. Furthermore, at the same level k_{c_1} is abruptly increasing in comparison to other hardening correction factors, which also adds to the effect of increasing the elastic regime. As a result of this, the damage accumulation is introduced later and later in the cyclic loading as the memory surface is reached later, and eventually a fully elastic state is present at tensile loadings for the given number of performed load cycles in the FE-analysis.

Only the tensile part of the flight representative loading cycle

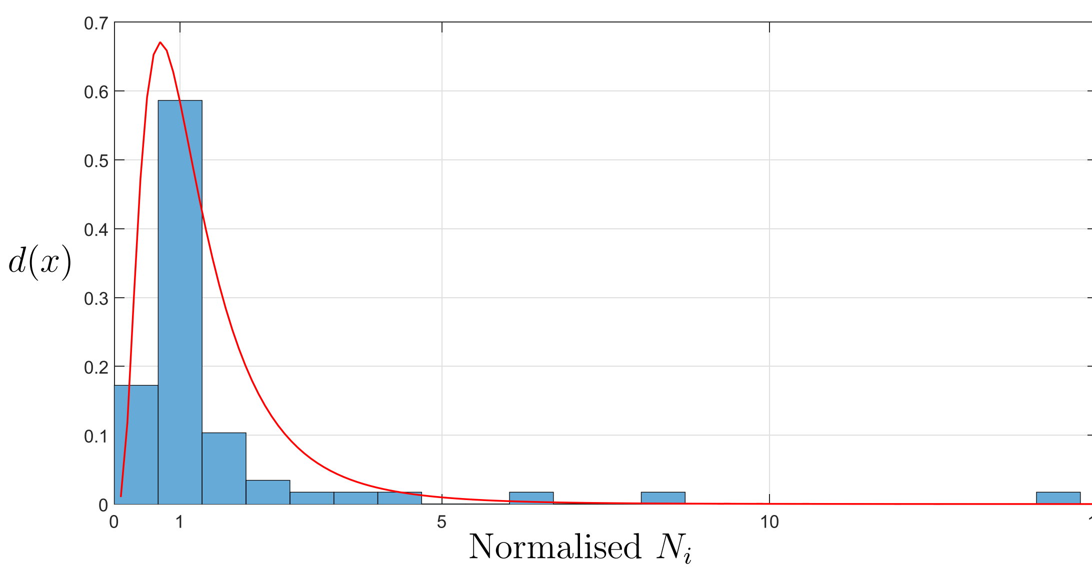

Fig. 13. Normalised histogram of the fatigue crack initiation life with a log-normal probability distribution.

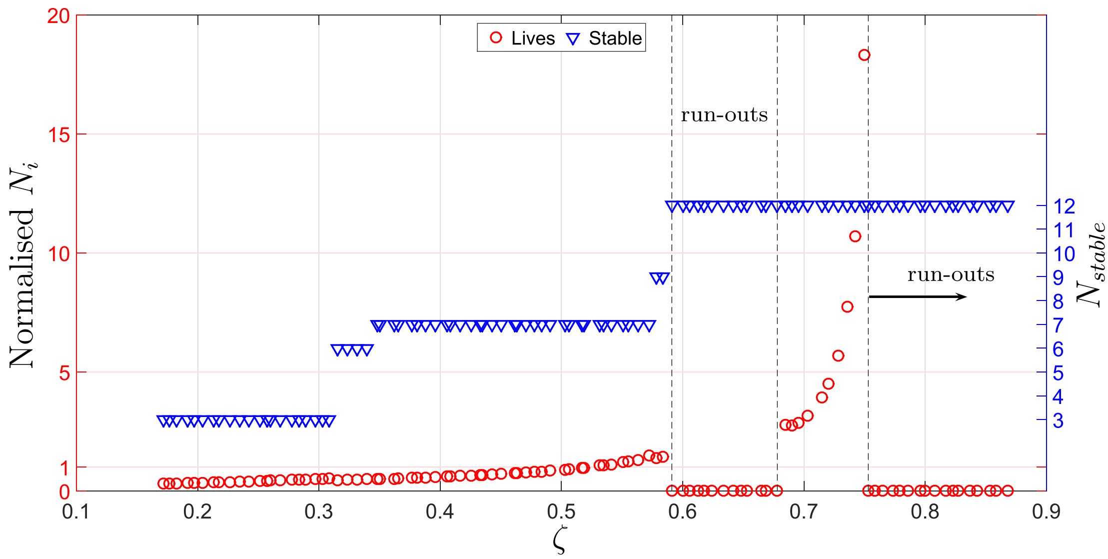

Fig. 14. Normalised fatigue crack initiation lives and the number of cycles to the stable state versus the input variable for the Monte-Carlo analysis with correction factor on the endurance limit.

Table 1
Statistical estimates of the two cases.

	First case		Second case	
	N_i	ζ	N_i	ζ
$\overline{\mu}$	0.8518	0.5003	0.6663	0.3775
$\overline{\sigma}$	0.2125	0.09183	0.07184	0.1225
c_v	0.2494	0.1835	0.1078	0.3246
Error estimate	0.2571	–	0.4517	–

contribute to the damage accumulation by using the adopted inelastic strain energy measure in Eq. (11), which can be reasonable from a micro-crack closure perspective. However, as the main loading in the applied load cycle is located in compression, it is also likely that damage will be accumulated for compressive loadings, *cf.* Fig. 12. A reason for including both tensile and compressive loadings is that in a general loading application, in which *e.g.* a pure compressive load case might be present, will also accumulate damage under corresponding conditions and initiate a fatigue crack.

In this work, only TMF loadings were considered, and for certain set of correction factors ($\zeta > 0.753$) only elastic states, or nearly elastic states, were obtained. To also accommodate for purely elastic load conditions, hence prevailing high-cycle fatigue conditions, the high-cycle fatigue life can be combined with the TMF life to generate a complete fatigue life response accounting for any type of loading situation. Thus, inclusion of a high-cycle fatigue term might be necessary to be incorporated into the already defined framework of the fatigue damage accumulation model to further increase the accuracy of the fatigue assessment. Furthermore, for these simulations, and those in the vicinity with a slightly lower input parameter value, the generated fatigue lives are a factor > 10 to the baseline life, *cf.* Fig. 10 and 14. Implying that there is no point in run the analysis longer than the twelve loading cycle applied, as a factor of 10 times nominal TMF lives are not to be considered as TMF load conditions. Nominal TMF lives for these applications and load levels are in the region of $1000 - 10000$ cycles, *cf.* [43,44].

The adopted constitutive model can sufficiently describe the material response under the applied flight representative load cycle, except for one thing, the dwell-time, *cf.* the baseline hysteresis loop at the stable damage state in Fig. 12 with the utilised flight relevant load cycle in Fig. 8. As the model is based on the Perzyna viscoplastic approach, which means that creep or inelastic flow only takes place when $f > 0$. Hence, the dwell-time period is located at relative low loads, which insinuates that no inelastic flow will be present at this period, and hence no creep deformation will occur. This is a drawback of the adopted model, and need to be handled for a better correlation to experimental observations. However, no experiments have here been compared to as the only interest lies in evaluating the scatter in constitutive parameters with respect to obtained fatigue crack initiation lives. Furthermore, as the loading is of an out-of-phase-TMF cycle, the evolution of the elastic stiffness is a function of temperature and consequently the trial stress in the predictor–corrector step of the stress update routine will also depend on the change in elastic stiffness with respect to temperature, *cf.* Ahmed and Hassan [51], accordingly to

$$\dot{\sigma}_{ij} = \mathbb{C}^e_{ijkl}\dot{\varepsilon}^e_{kl} + \dot{\mathbb{C}}^e_{ijkl}\varepsilon^e_{kl} \quad (19)$$

Due to cyclic loadings a synthetic ratcheting effect can be present in the constitutive model if this is not included depending on the type of hardening description that is adopted. In the case of an Armstrong-Frederick kinematic hardening description, which has been adopted in this work, the ratcheting phenomenon is overestimated and inherent to the model itself, and thus the synthetic ratcheting effect that would be present due to the temperature dependence in the predictor step is overtaken by the Armstrong-Frederick term. Implying that there is no need to include the temperature dependence in the predictor step, *i.e.* the latter part of Eq. (19).

6. Conclusions

In this paper the effect of scatter in constitutive parameters for the aerospace turbine rotor superalloy RR1000 on the TMF crack initiation life was evaluated by Monte-Carlo analysis and singular value decomposition, utilising a flight representative load cycle. It could be concluded that a small ‘scatter in’ on the constitutive parameters generates a very localised ‘scatter out’ effect on the fatigue crack initiation lives for the first case, when only considering correction factors (scatter) on the constitutive parameters. In addition, an obtained log-normal probability distribution of the predicted crack initiation lives showed a very high probability to obtain lives close to the baseline (mean) response. An even lower ‘scatter out’ effect could be seen in the second case, when the yield limit’s correction factor was also applied to the endurance limit in the fatigue damage model, fewer run-outs were also obtained. The use of singular value decomposition to investigate principal bases in constitutive parameter space has been proven to work well in defining physical representations of the constitutive parameters in conjunction with applied correction factors, for the number of parameters used in this study. As this study shows that a small 'scatter out' effect in the generated TMF lives are obtained, it also indicates that it can be used to assess the validity of the predicted fatigue lives based on inclusion of further constitutive parameter setups (future testing campaigns). A keypoint of high relevance for the gas turbine industry, since gathered material responses from previous and future testing campaigns can be incorporated with ease in this simple and industrially affordable concept to estimate and evaluate the fatigue life based on scatter in constitutive parameters (experimental data).

7. Data availability

The raw data as well as the processed data required to reproduce these findings cannot be shared due to confidentialities connected to intellectual properties tied to the partner company.

CRediT authorship contribution statement

Daniel Leidermark: Conceptualization, Methodology, Software, Validation, Formal analysis, Investigation, Writing - original draft, Writing - review & editing, Visualization, Funding acquisition. **James Rouse:** Conceptualization, Methodology, Software, Validation, Formal analysis, Investigation, Writing - original draft, Writing - review & editing, Visualization. **Benedikt Engel:** Writing - original draft. **Christopher Hyde:** Writing - original draft, Project administration, Funding acquisition. **Stephen Pattison:** Data curation. **Svjetlana Stekovic:** Project administration, Funding acquisition.

Declaration of Competing Interest

The authors declare that they have no known competing financial interests or personal relationships that could have appeared to influence the work reported in this paper.

Acknowledgements

The study has received funding from the Clean Sky 2 Joint Undertaking under the European Union's Horizon 2020 research and innovation programme under grant agreement No 686600.

References

[1] J. Tavernelli, L. Coffin, Experimental support for generalized equation predicting low cycle fatigue, Transactions of the American Society of Mechanical Engineers (ASME), Journal of Basic Engineering 84 (1962) 533–537.
[2] S. Manson, Discussion: Experimental support for generalized equation predicting low cycle fatigue, tavernelli and coffin, Transactions of the American Society of Mechanical Engineers (ASME), Journal of Basic Engineering 84 (1962) 537–541.
[3] D. Socie, J. Morrow, Review of contemporary approaches to fatigue damage analysis, in: J. Burke, V. Wiss (Eds.), Risk and Failure Analysis for Improved Performance and Reliability, Plenum Publication, New York, 1980, pp. 141–194.
[4] W. Findley, A theory for the effect of mean stress on fatigue of metals under combined torsion and axial load or bending, Journal of Engineering for Industry-Transactions of the ASME 81 (1959) 301–306.
[5] A. Karolczuk, E. Macha, A review of critical plane orientations in multiaxial fatigue failure criteria of metallic materials, International Journal of Fracture 134 (2005) 267–304.
[6] V. Bonnand, J. Chaboche, P. Gomez, P. Kanouté, D. Pacou, Investigation of multiaxial fatigue in the context of turboengine disc applications, International Journal of Fatigue 33 (2001) 1006–1016.
[7] R. Smith, P. Watson, T. Topper, A stress-strain parameter for the fatigue of metals, Journal of Materials 5 (1970) 767–778.
[8] W. Ostergren, A damage function and associated failure equations for predicting hold time and frequency effects in elevated temperature, low cycle fatigue, Journal of Testing and Evaluation 4 (1976) 327–339.
[9] D. Kulawinski, A. Weidner, S. Henkel, H. Biermann, Isothermal and thermo-mechanical fatigue behavior of the nickel base superalloy waspaloy under uniaxial and biaxial-planar loading, International Journal of Fatigue 81 (2015) 21–36.
[10] A. Fatemi, D.F. Socie, A critical plane to multiaxial fatigue damage including out-of-phase loading, Fatigue and Fracture of Engineering Materials and Structures 11 (1988) 149–165.
[11] J. Polák, J. Man, Initiation of stage i fatigue cracks - experiments and models, Procedia Engineering 101 (2015) 386–394.
[12] S. Suresh, Fatigue of Materials, second ed., Cambridge University Press, Cambridge, UK, 1998.
[13] U. Krupp, Fatigue Crack Propagation in Metals and Alloys, Wiley-VCH, 2007.
[14] J. Lemaitre, J.P. Sermage, One damage law for different mechanisms, Computational Mechanics 20 (1997) 84–88.
[15] J. Lemaitre, J.-L. Chaboche, Mechanics of Solid Materials, first ed., Cambridge University Press, Cambridge, UK, 1990.
[16] N. Ottosen, R. Stenström, M. Ristinmaa, Continuum approach to high-cycle fatigue modeling, International Journal of Fatigue 30 (2008) 996–1006.
[17] S. Lindström, Continuous-time, high-cycle fatigue model for nonproportional stress with validation for 7075-t6 aluminum alloy, International Journal of Fatigue 140 (2020), 105839.
[18] J.L. Chaboche, K. Dang Van, G. Cordier, Modelization of the strain memory effect on the cyclic hardening of 316 stainless steel, in: Proceedings of the 5th International Conference on Structural Mechanics in Reactor Technology, vol. L, 1979, p. L11/3.
[19] Y. Jiang, Fatigue criterion for general multiaxial loading, Fatigue and Fracture of Engineering Materials and Structures 23 (2000) 19–32.
[20] D. Leidermark, R. Eriksson, J. Rouse, C. Hyde, S. Stekovic, Thermomechanical fatigue crack initiation in disc alloys using a damage approach, MATEC Web Conferences 165 (2018) 19007.
[21] S. Beretta, S. Foletti, E. Rusconi, A. Riva, D. Socie, A log-normal format for failure probability under lcf: Concept, validation and definition of design curve, International Journal of Fatigue 82 (2016) 2–11.
[22] B. Lehmayr, S. Staudacher, A statistical model for scatter representation in stress life curves, Fatigue and Fracture of Engineering Materials and Structures 35 (2012) 347–358.
[23] S. Deyber, F. Alexandre, J. Vaissaud, A. Pineau, Probabilistic life of da 718 for aircraft engine disks, in: E. Loria (Ed.), Superalloys 718, 625, 706 and Derivatives, TMS (The Minerals, Metals & Materials Society), 2005, pp. 97–110.
[24] W. Musinski, D. McDowell, Microstructure-sensitive probabilistic modeling of hcf crack initiation and early crack growth in ni-base superalloy in100 notched components, International Journal of Fatigue 37 (2012) 41–53.
[25] S. Zhu, S. Foletti, S. Beretta, Probabilistic framework for multiaxial lcf assessment under material variability, International Journal of Fatigue 103 (2017) 371–385.
[26] S.-P. Zhu, Q. Liu, W. Peng, X.-C. Zhang, Computational-experimental approaches for fatigue reliability assessment of turbine bladed disks, International Journal of Mechanical Sciences 142–143 (2018) 502–517.
[27] S. Zhu, Q. Liu, J. Zhou, Z. Yu, Fatigue reliability assessment of turbine discs under multi-source uncertainties, Fatigue & Fracture of Engineering Materials & Structures 41 (2018) 1291–1305.
[28] X.-P. Niu, R.-Z. Wang, D. Liao, S.-P. Zhu, X.-C. Zhang, B. Keshtegara, Probabilistic modeling of uncertainties in fatigue reliability analysis of turbine bladed disks, International Journal of Fatigue 142 (2021), 105912.
[29] D. Leidermark, D. Aspenberg, D. Gustafsson, J. Moverare, K. Simonsson, The effect of random grain distributions on fatigue crack initiation in a notched coarse grained superalloy specimen, Computational Materials Science 51 (1) (2012) 273–280.
[30] B. Engel, J. Rouse, C. Hyde, W. Lavie, D. Leidermark, S. Stekovic, S. Williams, S. Pattison, B. Grant, M. Whittaker, J. Jones, R. Lancaster, H. Li, The prediction of crack propagation in coarse grain rr1000 using a unified modelling approach, International Journal of Fatigue 137 (2020), 105652.
[31] P. Perzyna, Thermodynamic theory of viscoplasticity, Advances in Applied Mechanics 11 (1971) 313–354.
[32] P.J. Armstrong, C.O. Frederick, A mathematical representation of the multiaxial bauschinger effect, Tech. rep., Berkeley Nuclear Laboratories, 1966.
[33] P.J. Armstrong, C.O. Frederick, A mathematical representation of the multiaxial bauschinger effect, Materials at High Temperatures 24 (2007) 1–26.
[34] J.L. Chacboche, Constitutive equations for cyclic plasticity and cyclic viscoplasticity, International Journal of Plasticity 5 (1989) 247–302.
[35] F. Odqvist, Creep stresses in a rotating disc, in: Proceedings of IV International Congress for Applied Mechanics, Cambridge, 1934, p. 228.
[36] N. Ottosen, M. Ristinmaa, The Mechanics of Constitutive Modeling, Elsevier, 2005.
[37] M. Kobayashi, N. Ohno, Implementation of cyclic plasticity models based on a general form of kinematic hardening, International Journal for Numerical Methods in Engineering 53 (2002) 2217–2238.
[38] A.H. Cottrell, Dislocations and Plastic Flow in Crystals, first ed., Oxford University Press, Oxford, U.K., 1953.
[39] J. Rouse, C. Hyde, W. Sun, T. Hyde, Comparison of several optimisation strategies for the determination of material constants in the chaboche visco-plasticity model, Journal of Strain Analysis in Engineering Design 48 (2013) 347–363.
[40] S.T. Kyaw, J.P. Rouse, J. Lu, W. Sun, Determination of material parameters for a unified viscoplasticity-damage model for a p91 power plant steel, International Journal of Mechanical Sciences 115–116 (2016) 168–179.
[41] J.P. Rouse, P. Zacharzewski, C.J. Hyde, R. Jefferson-Loveday, A. Morris, S.T. Kyaw, A case study investigation into the effects of spatially dependent convection coefficients on the fatigue response of a power plant header component, International Journal of Fatigue 113.
[42] K. Pearson, On lines and planes of closest fit to systems of points in space, Philosophical Magazine 2 (1901) 559–572, https://doi.org/10.1080/14786440109462720.

[43] R. Lancaster, M. Whittaker, S. Williams, A review of thermo-mechanical fatigue behaviour in polycrystalline nickel superalloys for turbine disc applications, Materials at High Temperatures 30 (2013) 2–12.
[44] R.-Z. Wang, S.-P. Zhu, J. Wang, X.-C. Zhang, S.-T. Tu, C.-C. Zhang, High temperature fatigue and creep-fatigue behaviors in a ni-based superalloy: Damage mechanisms and life assessment, International Journal of Fatigue 118 (2019) 8–21.
[45] D. Leidermark, K. Simonsson, Procedures for handling computationally heavy cyclic load cases with application to a disc alloy material, Materials at High Temperatures 36 (2019) 447–458.
[46] Matlab r2015a, Tech. rep., The MathWorks Inc., Natick, 2018.
[47] N. Stander, W. Roux, T. Goel, T. Eggleston, K. Craig, LS-OPT User's Manual, Livermore Software Technology Corporation, Livermore, 2010.
[48] J.O. Hallquist, LS-DYNA Theory Manual, Livermore Software Technology Corporation, Livermore, 2006.
[49] J. Moverare, S. Johansson, R. Reed, Deformation and damage mechanisms during thermal-mechanical fatigue of a single-crystal superalloy, Acta Materialia 57 (2009) 2266–2276.
[50] O.M.D.M. Messé, S. Stekovic, M. Hardy, C.M.F. Rae, Investigation on fatigue crack interaction with grain orientation during tmf tests in nickel-base superalloy, Advanced Materials Research 891–892 (2014) 1289–1294.
[51] R. Ahmed, T. Hassan, Constitutive modeling for thermo-mechanical low-cycle fatigue-creep stress-strain responses of haynes 230, International Journal of Solids and Structures 126–127 (2017) 122–139.